Clim Dyn (2016) 47:951–965
DOI 10.1007/s00382-015-2882-9

ORIGINAL ARTICLE

Spatial stabilization and intensification of moistening and drying rate patterns under future climate change

Yann Chavaillaz[1] · Sylvie Joussaume[1] · Sandrine Bony[2] · Pascale Braconnot[1]

Received: 19 April 2015 / Accepted: 16 October 2015 / Published online: 26 October 2015

Abstract Precipitation projections are usually presented as the change in precipitation between a fixed current baseline and a particular time in the future. However, upcoming generations will be affected in a way probably more related to the moving trend in precipitation patterns, i.e. to the rate and the persistence of regional precipitation changes from one generation to the next, than to changes relative to a fixed current baseline. In this perspective, we propose an alternative characterization of the future precipitation changes predicted by general circulation models, focusing on the precipitation difference between two subsequent 20-year periods. We show that in a business-as-usual emission pathway, the moistening and drying rates increase by 30–40 %, both over land and ocean. As we move further over the twenty-first century, more regions exhibit a significant rate of precipitation change, while the patterns become geographically stationary and the trends persistent. The stabilization of the geographical rate patterns that occurs despite the acceleration of global warming can be physically explained: it results from the increasing contribution of thermodynamic processes compared to dynamic processes in the control of precipitation change. We show that such an evolution is already noticeable over the last decades, and that it could be reversed if strong mitigation policies were quickly implemented. The combination of intensification and increasing persistence of precipitation rate patterns may affect the way human societies and natural ecosystems adapt to climate change, especially in the Mediterranean basin, in Central America, in South Asia and in the Arctic.

Keywords Climate change · CMIP5 simulations · Persistent rate patterns · Rate of precipitation change · Spatial stabilization

✉ Yann Chavaillaz
yann.chavaillaz@lsce.ipsl.fr

[1] Laboratoire des Sciences du Climat et de l'Environnement (LSCE-IPSL), CEA/CNRS/UVSQ, Orme des Merisiers, 91191 Gif-sur-Yvette Cedex, France

[2] Laboratoire de Météorologie Dynamique (LMD-IPSL), CNRS/Université Pierre et Marie Curie, 4, Place Jussieu, 75252 Paris, France

1 Scientific context

Since the mid-twentieth century, the oceans and the atmosphere have been experiencing unprecedented warming for the past 1400 years (Masson-Delmotte et al. 2013). Global warming is expected to continue over the twenty-first century, and will be associated with a proportional increase in global precipitation estimated at 1– 3 %/°C (Collins et al. 2013). This global positive trend will however be associated with large regional disparities, such as a growing contrast between regions of moisture convergence and divergence, and between dry and wet seasons (Chou et al. 2013; Collins et al. 2013; Liu and Allan 2013). It is understood as a consequence of the Clausius–Clapeyron relationship, the increased transport of water vapor from the tropics, and partly of the *likely* slowdown of the Hadley-Walker circulation (Allan 2012; Bony et al. 2013; Chadwick et al. 2013; Collins et al. 2013; Vecchi and Soden 2007). These conclusions were drawn by focusing on changes between the future and a fixed current baseline that usually corresponds to the 1986–2005 period.

In an attempt to present precipitation projections in a way that is more relevant for impact assessments, several studies focused on the time of emergence of precipitation signals (e.g. Giorgi and Bi 2009; Mahlstein et al. 2012;

Maraun 2013; Mora et al. 2013). However, natural and human systems have a limited capacity to adapt to environmental changes, and are strongly dependent on how fast climatic conditions evolve (Settele et al. 2014). Rapid changes threaten biodiversity and ecosystem function (Chapin et al. 2000; Dawson et al. 2011). Adaptation planning and implementation are also continuous processes, driven by the rate of climate change (Klein et al. 2014).

Therefore, impact studies and adaptation strategies would benefit from additional insights if the precipitation projections from climate models were presented in a way that characterizes the rate of change of regional precipitation, rather than the absolute change relative to a fixed reference. The evolution (or "path") of precipitation changes over the twenty-first century is likely to depend on the forcing pathway. However, it may also depend on different factors internal to the climate system, since their relative importance in controlling the regional patterns of precipitation change may evolve as global warming proceeds. Unraveling and physically understanding these factors could help extract some robust information from climate models, which would be highly welcome given the large uncertainties associated with regional rainfall projections.

In this perspective, this study proposes an alternative characterization of the regional precipitation changes projected by general circulation models (GCMs), which focuses on the evolution of the rate of precipitation change with time. For this purpose, we consider a running n-year baseline. For each year, the rate of change is defined as the change in annual mean precipitation that should be expected over the upcoming n years relative to the n previous years. Chavaillaz et al (submitted) conducted a similar analysis for temperature changes over the twenty-first century, and showed how fast the climatological standards corresponding to the n-year running baseline will be outdated. Recently, Ji et al. (2014) and Smith et al. (2015) analyzed the rate of near-surface air temperature change, describing a derivative of the temperature change, and focusing on the historical period and on the next few decades respectively. In the present study, we assess the rate of precipitation changes over the entire twenty-first century, and identify the persistence of robust precipitation trends that could lead to substantial impacts on human societies and natural ecosystems.

Section 2 defines indicators and describes the experiment design. Section 3 focuses on the representation of our indicators at the global scale, as well as on regions relevant for their robust changes among GCMs and for their persistent trends over the twenty-first century. Section 4 highlights physical processes causing the persistence of precipitation trends. Finally, Sect. 5 summarizes our outcomes, discusses the limitations of the study, and draws some conclusions for impacts and adaptation studies.

2 Methods

2.1 Definition of precipitation indicators

For the purpose of the study, the length of the running baseline is arbitrarily set to 20 years. Climate standards are therefore defined over a two-decade, as we move the window towards the subsequent period. This timescale is an appropriate option to properly assess the evolution of the rate of change, to limit the impact of natural variability (e.g. Liebmann et al. 2010), and to be consistent with IPCC assessments and requirements of European climate services (Street et al. 2015).

We denote ΔP_{20} as the *rate of precipitation change*, which is characterized by the difference of the annual mean precipitation between two consecutive 20-year periods. It is expressed in millimeters per day per two-decade:

$$\Delta P_{20}(t) = \langle P \rangle_{t,t+20} - \langle P \rangle_{t-20,t} \tag{2.1}$$

where $\langle \cdot \rangle$ is the temporal average of annual values over 20 years. The current period is arbitrarily chosen in 1995 because of its central position in the period most commonly considered as a reference for the late historical period (1986–2005), and because the later year taken into account in the calculation is the present day ($t + 20 = 2015$). This definition implies that the evolution of our indicator is influenced by future emission scenarios since 1986.

In contrast to temperature change, which is mainly positive, the projected precipitation change consists of an increase in some regions and a decrease in some others. Regions with an increase or a decrease are not necessarily the same through time. For each year and for each realization of each GCM, grid cells in which ΔP_{20} is positive are separated from the grid cells in which it is negative. Spatially averaging all positive (negative) differences defines the *moistening (drying) rate*, denoted ΔP_{20}^{+} (ΔP_{20}^{-}). The drying rate is defined so that it is positive when precipitation decreases. At each location (i, j) and for each year t:

$$\begin{cases} \Delta P_{20,i,j}^{+} = \Delta P_{20,i,j} \text{ if } \Delta P_{20,i,j} \geq 0 \\ \Delta P_{20,i,j}^{-} = -\Delta P_{20,i,j} \text{ if } \Delta P_{20,i,j} < 0 \\ \Delta P_{20}^{+(-)} = \left[\Delta P_{20,i,j}^{+(-)}\right]_{i,j} \end{cases} \tag{2.2}$$

where i and j are indices of longitude and latitude, respectively. $[\cdot]_{i,j}$ then represents the area weighted spatial average.

The *1995-ratio of the moistening (drying) rate* allows comparing the future amplitude of each rate with current values. It is computed as follows:

$$R_{+(-)}(t) = \frac{\Delta P_{20}^{+(-)}(t)}{\Delta P_{20}^{+(-)}(1995)} \tag{2.3}$$

Table 1 Number of realizations taken into account per model and pathway

CMIP5 GCMs	#realizations		
	historical	rcp2.6	rcp8.5
ACCESS1-0	1	0	1
bcc-csm1-1	1	1	1
BNU-ESM	1	1	1
CanESM2	5	5	5
CCSM4	6	6	6
CMCC-CM	1	0	1
CNRM-CM5	4	1	4
CSIRO-Mk3.6.0	1	1	1
FGOALS-s2	3	1	3
GFDL-CM3	1	1	1
GISS-E2-R	1	1	1
HadGEM2-ES	4	4	4
inmcm4	1	0	1
IPSL-CM5A-LR	4	4	4
MIROC5	3	3	3
MPI-ESM-LR	3	3	3
MRI-CGCM3	1	1	1
Nor-ESM1-M	1	1	1
	40	34	40

See Flato et al. (2013) for model characteristics and references

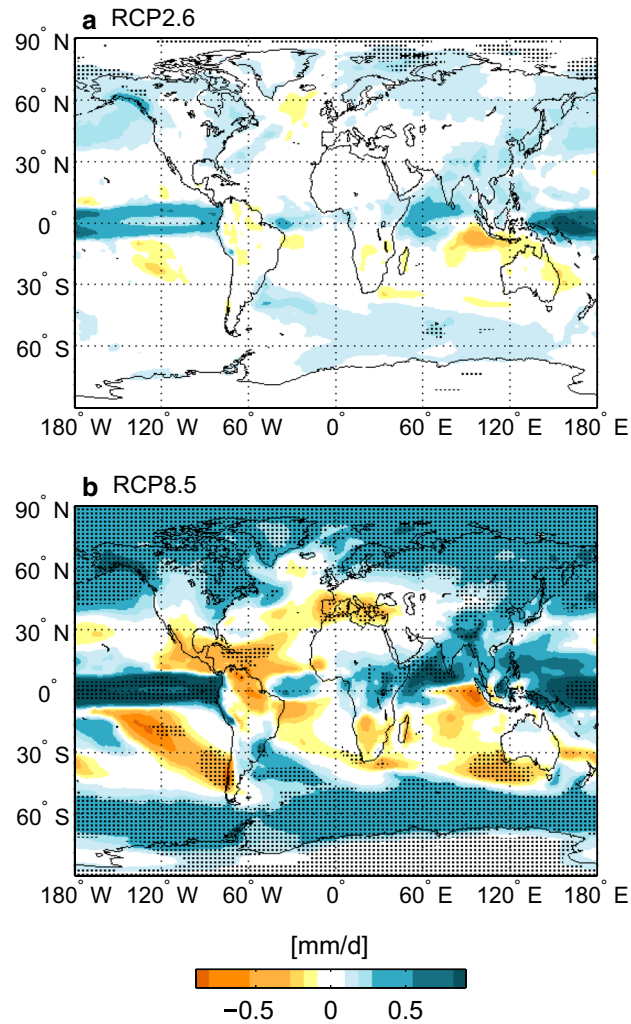

Fig. 1 Multi-model mean of the absolute change of annual precipitation between (1986–2005) and (2081–2100) for **a** RCP2.6 and **b** RCP8.5. *Blue* (*yellow*) patterns highlight an increase (decrease) in precipitation. *Dotted areas* denote where at least 90 % of GCMs agree on the sign of the change and where the change exceeds at least two times the internal variability (Collins et al. 2013, p. 1041). All GCMs and all realizations cited in Table 1 are taken into account in the calculation

The *fraction of moistening (drying) regions*, denoted $\Pi_+(\Pi_-)$, is defined as the fraction of regions where ΔP_{20} is positive (negative). Moistening and drying rates are additive when weighted by Π_+ and Π_- respectively (see "Appendix 1").

Aside from modifications of Π_+ and Π_-, some regions can obviously switch over time from a drying trend to a moistening trend or vice versa. The *fraction of switching regions* is then defined as the fraction of regions where ΔP_{20} has the opposite sign to the previous 20-year period:

$$\Pi_{s20}(t) = F(\Delta P_{20}(t) \cdot \Delta P_{20}(t-20) < 0) \tag{2.4}$$

This indicator characterizes the degree of persistence of moistening and drying trends in a given region. The lower Π_{s20}, the greater the persistence.

2.2 Multi-model analysis

In this study, we selected simulations from the fifth Coupled Model Intercomparison Project (CMIP5) (Taylor et al. 2011) performed by 18 GCMs. For institutes with several models or versions, only the one having the most realizations is selected. Each realization is included with the intention of better evaluating internal variability (Deser et al. 2010). However, in order to equally represent every model in multi-model mean values, each realization is weighted with a factor of $1/R_l$, where R_l is the number of realizations for the model l.

Data of each model and each realization is first regridded to the CCSM4 model grid (1.25° × 0.9375°) in order to be homogenous (Flato et al. 2013). Indicators are then computed in each grid cell and averaged over the focused region for each run, before carrying out multi-model means.

Two sources of uncertainty are partitioned in our analysis: the *natural* variability of the climate system (i.e. internal variability and natural forcing) and the *inter-model* variability. We make the assumption that these uncertainties

are additive and their sum represents the total variability of our indicators, which is true as a first approximation (see "Appendix 2"; Kirtman et al. 2013; Hawkins and Sutton 2009, 2011).

Climate projections were performed for four Representative Concentration Pathways (RCPs) (Meinshausen et al. 2011). We mainly focus on RCP8.5, since this pathway would cause the most substantial precipitation changes and represents one of the possible scenario in the absence of immediate implementation of mitigation measures. RCP2.6 is a possible pathway in the case of massive mitigation measures (Collins et al. 2013). Occasional comparisons between both RCPs are undertaken where appropriate. These pathways may not be realistic but are useful in analyzing the potential sensitivity of our outcomes. For RCP8.5 (RCP2.6), an ensemble of forty (thirty-four) runs is selected (see Table 1).

By the end of the century (2081–2100), every GCM predicts a global increase in precipitation compared to the current period (here chosen as 1986–2005). Figure 1 illustrates its multi-model mean projected for both RCP2.6 and RCP8.5. This illustrates the increasing contrast between moisture divergence (subtropics) and convergence regions (tropics and mid- to high-latitudes). The intensity of precipitation change scales with the temperature change amplitude. The collection of GCMs chosen in this study makes us draw similar conclusions than the IPCC AR5 report (Collins et al. 2013).

3 Global patterns of precipitation indicators

3.1 Rate of precipitation change

Spatial modifications of ΔP_{20} under RCP8.5 are illustrated in Fig. 2. In 1970, regions with a significant rate of change across GCMs and compared to internal variability were virtually nonexistent. They tend to equally expand over land and ocean, when we move further through time. Indeed, the fraction of land affected by a significant rate goes from around 8 % in 1995 to 28 % in 2080, while the corresponding fraction of ocean goes from 10 to 25 %.

Figure 2 also shows that the rate of precipitation change strongly increases over the century. The global average amplitude of this indicator exhibit a similar trend (red curve of Fig. 3a). During the historical period, it displays an oscillation around zero, and then a large increase for all GCMs with two peaks around 2010 and 2080. This evolution corresponds to an acceleration of precipitation change during the twenty-first century, and is strongly linked with the evolution of the warming rate (ΔT_{20}), which follows the radiative forcing evolution constructed in the RCP design (Chavaillaz et al, submitted). By the end of the century, the global average of ΔP_{20} tends to stabilize around 0.05 millimeters per day per two-decade, which leads to a doubling compared with 1995-values. This evolution corresponds to a temporal average of $\Delta P_{20}/\Delta T_{20}$ of around 2.3 ± 1.0 percent per Kelvin over the entire twenty-first century (using a one σ-interval). It is consistent with the strong correlation of the absolute change of precipitation with the absolute change of temperature (Collins et al. 2013), and shows that this relation is preserved using a running baseline.

In contrast, RCP2.6 displays a common evolution with RCP8.5 in the current period, but rapidly returns to a historical regime consisting of a rate of precipitation change close to zero (blue curve of Fig. 3a).

Figure 3b depicts the evolution of ΔP_{20} given by three observational datasets compared with the corresponding multi-model mean values masked on the same grid cells. Rate amplitudes are larger than in the GCMs, which is consistent with Zhang et al. (2007) and Allan et al. (2014). While they are in phase with one another, the three different observed ΔP_{20} exhibit a slight phase difference of about 20 years with simulated results. It can be due to a combination of both forced and unforced variabilities. On one hand, the phase difference can be due to internal decadal variability in the Pacific and Atlantic that determines fluctuations in precipitation over land (Liu and Allan 2013). On the other hand, the definition of ΔP_{20} considers differences between 20-year means, and therefore smoothes oscillations due to natural variability. Similar discrepancies are moreover displayed in the ΔT_{20} evolution, and were found to be linked to forcing (Chavaillaz et al. submitted). These discrepancies are further discussed in Sect. 5.

The global evolution of ΔP_{20} conceals a moistening trend in some regions and a drying trend in some others. It is unsuitable to assess impacts of precipitation change at the regional scale. Drying and moistening regions relative to ΔP_{20} are thus separated in the next subsection.

3.2 Distinction between moistening and drying rates

Moistening and drying trends keep accelerating by the end of the century under RCP8.5 (Fig. 4a, b), despite the decreasing acceleration of precipitation change at the global scale. In other words, the peak of ΔP_{20} by 2080 (red curve of Fig. 3a) conceals a continuous acceleration of drying and moistening rate patterns. This acceleration in both drying and moistening is predicted by each GCM. It corresponds to a 1995-ratio of the moistening rate R_+ reaching 1.40 ± 0.10 and a 1995-ratio of the drying rate R_- of 1.26 ± 0.09 by 2080 (using a $\pm\sigma$-interval of the total variability). Both moistening and drying rates are smaller over land surfaces than over oceans, but follow a similar evolution as at the global scale over the entire twenty-first century (not shown). Indeed, the 1995-ratio of both rates show similar range (see Table 2).

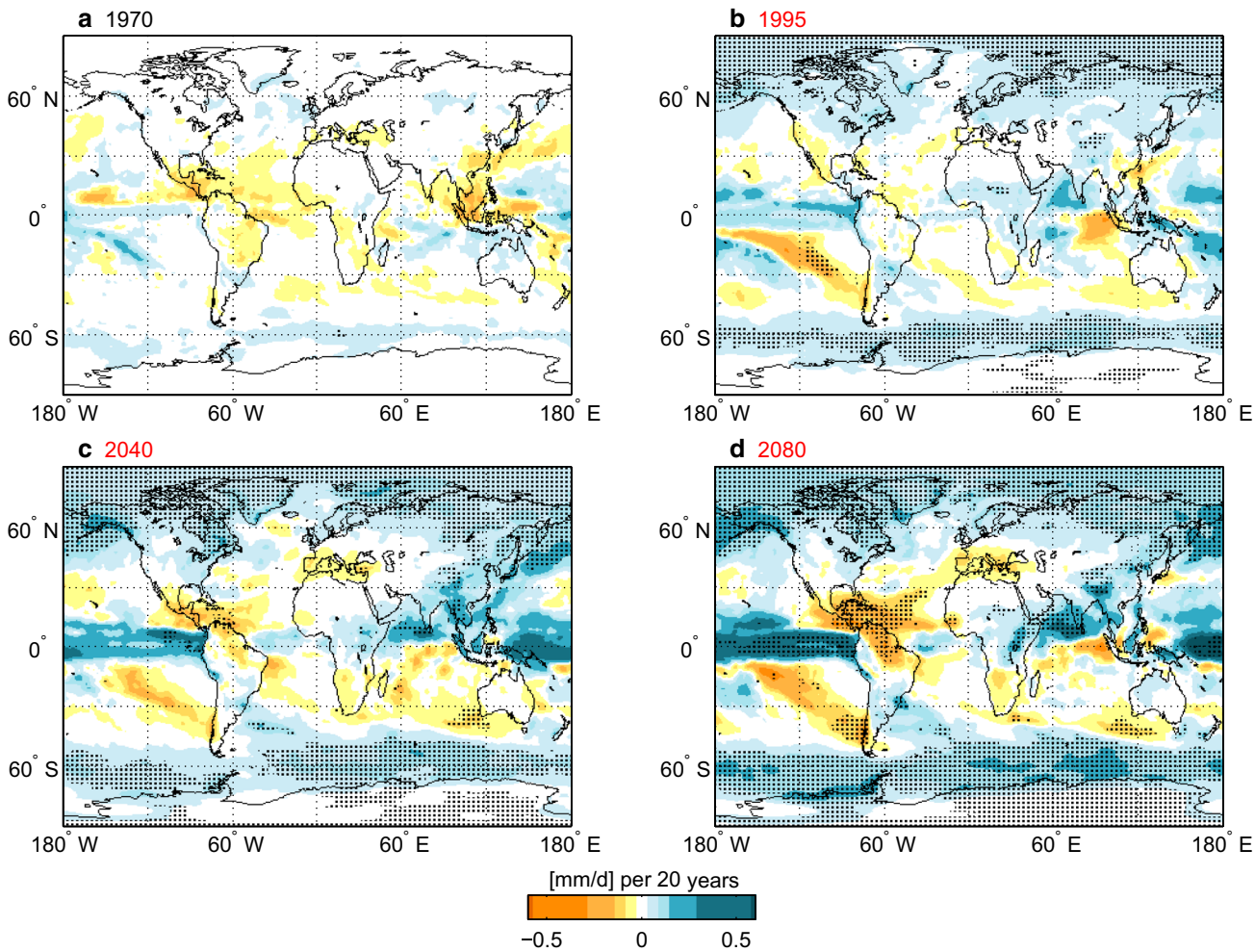

Fig. 2 Multi-model mean of the annual rate of precipitation change ΔP_{20} **a** in 1970, **b** in 1995, **c** in 2040 and **d** in 2080 under the RCP8.5 scenario. For instance, the 2040 map represents the precipitation change between (2021–2040) and (2041–2060). *Blue* (*yellow*) patterns highlight a positive (negative) rate of precipitation change, i.e. a moistening (drying) trend. *Dotted areas* denote where at least 75 % of GCMs agree on the sign of the change, and where the change exceeds at least one time the internal variability (similar to Collins et al. 2013, p. 1041)

The fraction of moistening regions Π_+ is close to 50 % during the whole of the historical period, and almost tends to have currently reached its maximum value (Fig. 4c). This equal representation of drying and moistening regions offsets both drying and moistening rates (about 0.12 mm per day on Fig. 4a, b), and leads to negligible values of ΔP_{20} during the historical period (Fig. 3a). Π_+ is predicted to be close to its maximum value over the entire twenty-first century under RCP8.5 (59.1 ± 3.3 %). This constant ratio of about 60 % of moistening regions versus about 40 % of drying regions is also displayed over land surfaces and oceans separately (not shown).

In comparison, RCP2.6 follows RCP8.5 evolution until the current period, but goes back to a 50/50 % ratio by 2050 with no significant increase in both drying and moistening rates, similar to the historical regime.

A constant fraction Π_+ does not mean that these areas remain the same over time. The drying and moistening rate patterns might spatially vary, even though their respective fractional area remains identical. The following subsection aims to determine which regions do come out with a significant rate pattern persisting over the century.

3.3 Towards stabilization of moistening and drying regions

Figure 5 displays the sign of the rate of precipitation change ΔP_{20}, instead of its amplitude (Fig. 2). Hatched regions show that some moistening and drying regions do change over time under RCP8.5. However, as we move further over the twenty-first century, a large decrease is displayed in the spatial extent of switching regions. This already occurs

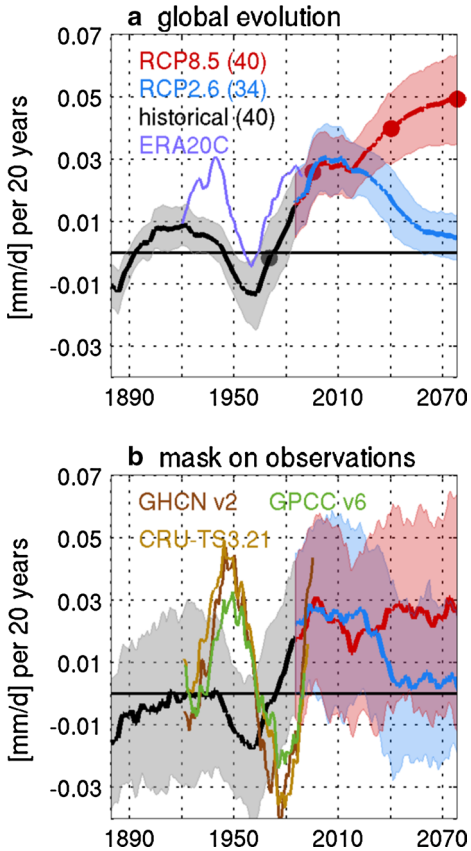

Fig. 3 Spatial mean evolution of ΔP_{20} under RCP8.5, RCP2.6 and the historical experiment **a** at the global scale with reanalysis (Poli et al. 2013), and **b** with a mask on observation datasets (Vose et al. 1992; Harris et al. 2014; Becker et al. 2013). *Shades* represent the standard deviation due to the total year-to-year variability (natural and inter-model). Each *bold dot* corresponds to a map in Fig. 2. The number of runs is given in parenthesis

between 1970 and 1995 (Fig. 5a, b). During the whole of the historical period, the fraction of switching regions is about 65 % (64.7 ± 4.2 %) at the global scale, then goes to 57.3 ± 4.6 % in 1995 to finally drop to 40.7 ± 4.7 % by 2080 (Fig. 6). This substantial decrease is displayed by the entire panel of GCMs, and stays similar when land surfaces and oceans are separated (not shown).

The decline of switching regions logically results in an increase in the fraction of regions experiencing a rate pattern of the same sign over the century. Therefore, moistening and drying rate patterns are not only experiencing a substantial intensification, but they are also projected to persist more over the same regions as we move further over the twenty-first century.

On the contrary, RCP2.6 highlights a return to historical regime as previously explained: after a sudden decrease in the fraction of switching regions until 2010 (i.e. for the 2011–2030 period), it is predicted to go back to typical values of the twentieth century (blue curve of Fig. 6). This is why all the phenomena described here under RCP8.5 (increase in rates, stable predominance of moistening regions and spatial stabilization of significant rate patterns) might not happen in case of immediate strong mitigation policies.

3.4 Focus on regions with robust information

The globe can be divided in different regions defined in the IPCC SREX report (Seneviratne et al. 2012). Four of these regions are here selected amongst those exhibiting a significant (Fig. 2) and persistent (Fig. 5) trend of precipitation change under RCP8.5, with the aim of extracting robust information relevant to impact studies. They are

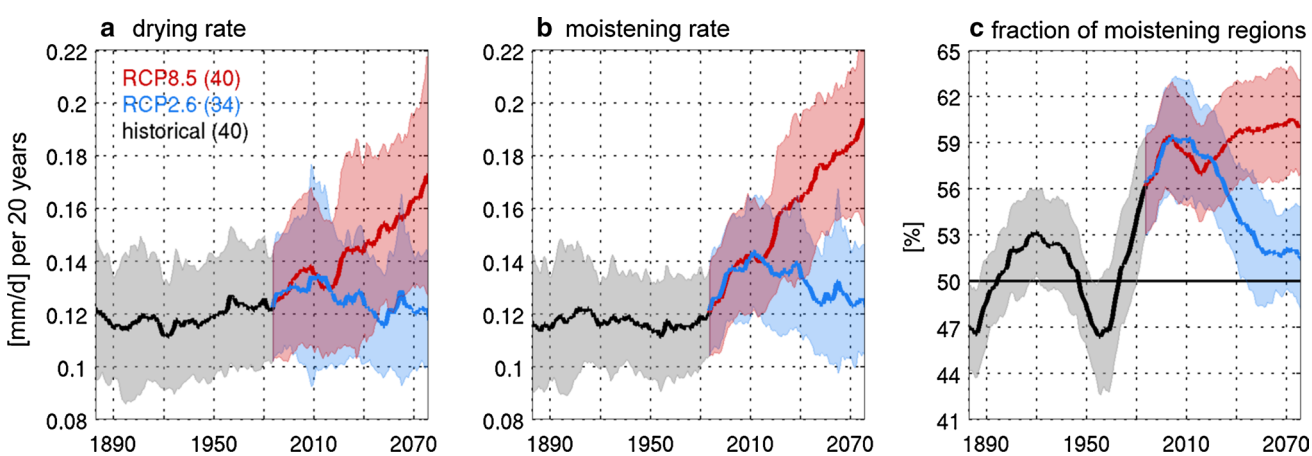

Fig. 4 Multi-model mean evolution of **a** the drying rate ΔP_{20}^{-}, **b** the moistening rate ΔP_{20}^{+} and **c** the fraction of moistening regions Π_{+} at the global scale under RCP8.5, RCP2.6 and the historical experiment. *Shades* represent the standard deviation due to the total year-to-year variability (natural and inter-model)

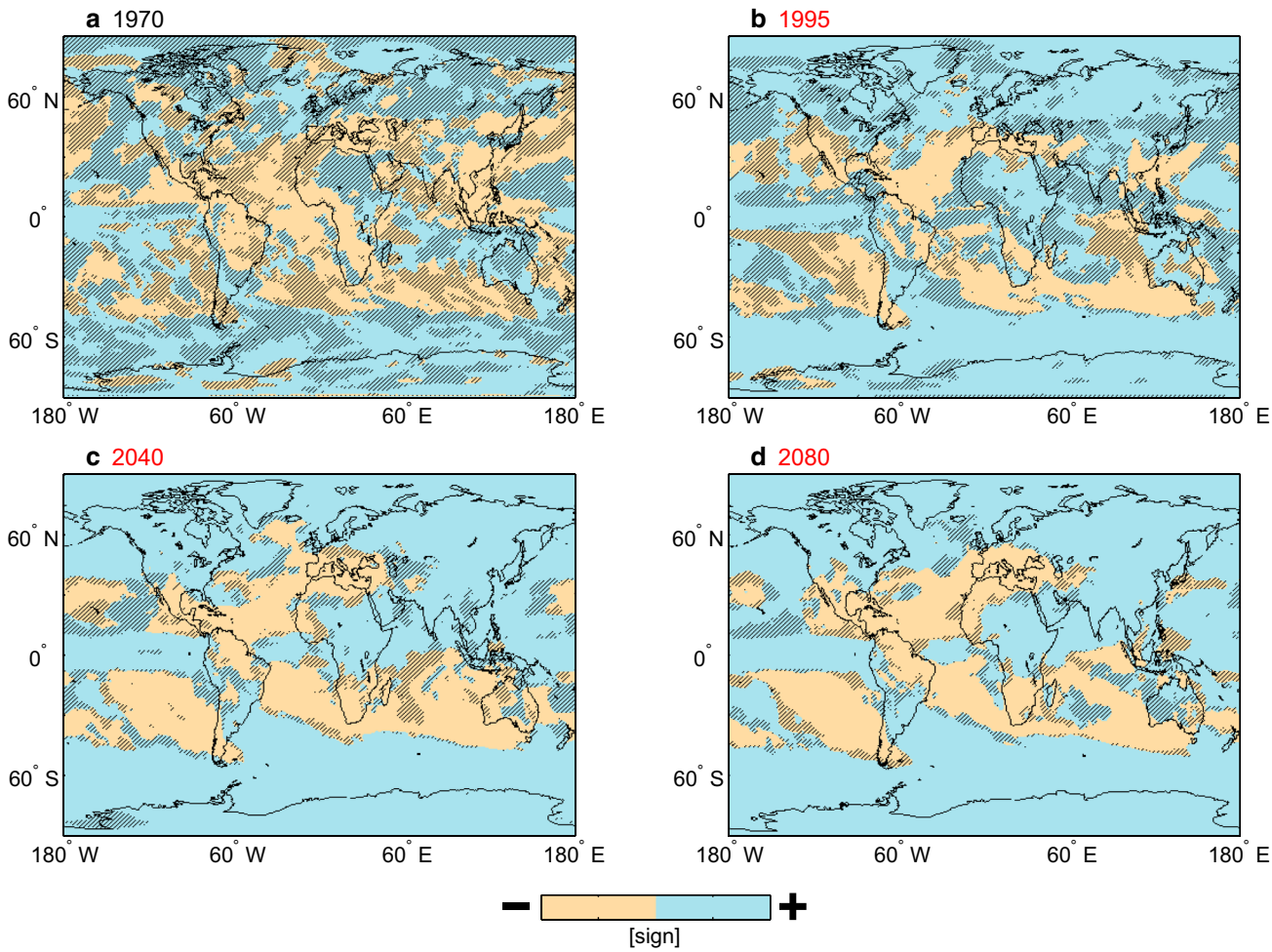

Fig. 5 Sign of the multi-model mean of the rate of precipitation change ΔP_{20} **a** in 1970, **b** in 1995, **c** in 2040 and **d** in 2080 under the RCP8.5 scenario. For instance, the 2040 map represents the sign of precipitation change between (2021–2040) and (2041–2060). *Blue* (*yellow*) patterns highlight a positive (negative) rate of precipitation change, i.e. a moistening (drying) trend. *Hatched areas* represent regions having the opposite sign of ΔP_{20} compared to 20 years before (i.e. switching regions)

also part of those facing important challenges and/or a high population density. The Mediterranean basin (MED) and Central America (CAM) highlight a drying trend, whereas South Asia (SAS) and the Arctic (ARC) exhibit a moistening trend. Their boundaries are described in Table 2 and on Fig. 7a. In these regions, the inter-model variability accounts for a lower fraction of the total variability (around 50 %) than at the global scale (around 65 %), which confirms the consensus and the robustness of the trends (not shown). We compare here the regional evolution of rates to their global evolution.

The precipitation amount greatly varies amongst regions. Normalized moistening and drying rates are analyzed here for relevant comparison, and are expressed as a percentage:

$$\widetilde{\Delta} P_{20}^{+(-)} = \frac{\Delta P_{20}^{+(-)}}{\langle P \rangle_{t-20,t}} \cdot 100 \tag{3.1}$$

Compared to the global evolution, each region highlights larger normalized moistening and drying rates over the entire twenty-first century (Fig. 7b, c). Two thirds of the GCMs agree that $\widetilde{\Delta} P_{20}^{+}$ is smaller in ARC compared to SAS. In 2080, the 1995-ratio also exhibits larger values in each region than at the global scale. According to 60 % of the GCMs, a larger 1995-ratio is displayed in CAM with comparison with MED, despite a reversed ranking regarding $\widetilde{\Delta} P_{20}^{-}$ values. The drying trend in CAM is projected to be twice as fast by 2080 than it is currently (from about 5.5 % in 1995 to 11 % in 2080, corresponding to a 1995-ratio of 2.01 ± 0.58, see Table 2).

Low-frequency variability in Fig. 7b, c should not be misinterpreted. Indeed, oscillations in the multi-model mean regional evolution of rates result from unforced oscillations due to inherent internal variability of a specific GCM, or from a combination of oscillations caused by the entire collection of GCMs (not shown).

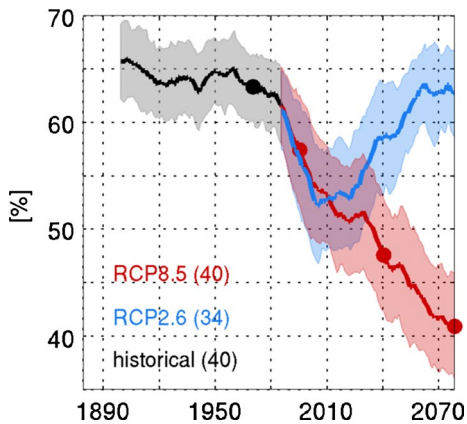

Fig. 6 Multi-model mean evolution of the fraction of switching regions Π_{s20} at the global scale under RCP8.5, RCP2.6 and the historical experiment. *Shades* represent the standard deviation due to the total year-to-year variability (natural and inter-model). Each *bold dot* corresponds to a map in Fig. 5. The number of runs is given in parenthesis

Analyses conducted for DJF, MAM, JJA and SON seasons show that the regional evolution of annual moistening and drying rates is often dominated by a specific season (not shown). In MED, the annual evolution emphasizes the intensification of the JJA drought. In CAM, it depends on the attenuation of the JJA wet season (consistent with Neelin et al. 2006). In SAS, it is consistent with a later retreat of the monsoon in September. Finally, in ARC, all seasons affect the annual evolution, with a slight dominance of DJF.

4 Physical understanding of the spatial stabilization

As shown above, the more we move into the twenty-first century, the more significant rates of precipitation change persist over the same regions under RCP8.5. This result is suggested by all the selected models, and it occurs over both land and ocean. It is thus not primarily related to land-surface processes. Is this robust result simply due to forcing, or is it rather due to other effects inherent to the climate system? To answer this, we analyze the components of ΔP_{20}, ΔP_{20}^{+} and ΔP_{20}^{-}, which are due to thermodynamic and dynamic processes. For convenience of the analysis, we first perform this decomposition over ocean regions, and then the generalization of the interpretation to land regions will be assessed.

4.1 Thermodynamic and dynamic decomposition over ocean

Based on Held and Soden (2006) and Bony et al. (2013), the thermodynamic and dynamic components can be

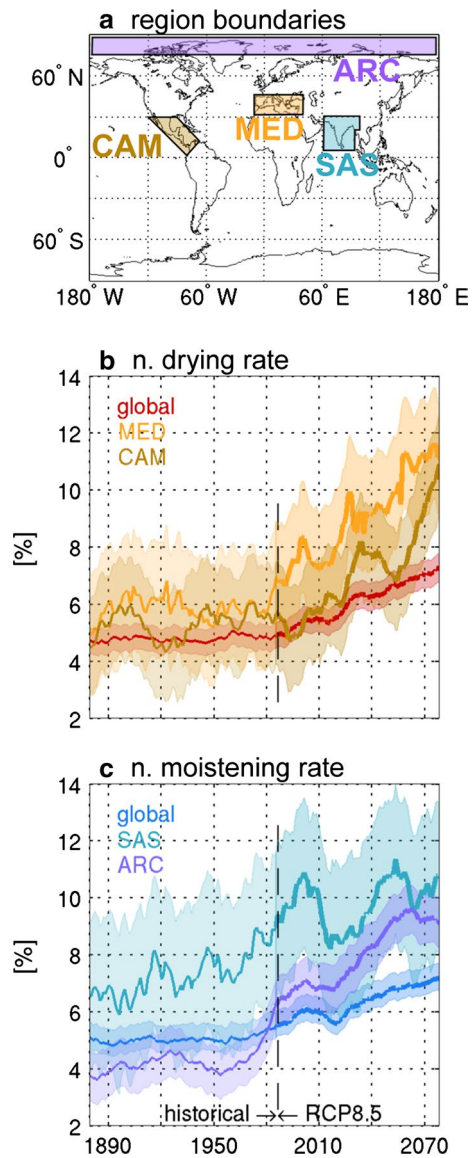

Fig. 7 **a** Spatial boundaries of SREX regions selected for the analysis. Multi-model mean evolution of **b** the normalized drying rate $\widetilde{\Delta P}_{20}^{-}$ and **c** the normalized moistening rate $\widetilde{\Delta P}_{20}^{+}$ at the global scale and in SREX regions under the historical experiment and RCP8.5. *Shades* represent the standard deviation due to the natural variability

expressed in each grid cell, run, GCM and time-step as follows :

$$\begin{cases} \Delta P_{20}^{th} = \Delta E_{20} + \alpha(\langle P \rangle - \langle E \rangle)\Delta T_{20} \\ \Delta P_{20}^{dyn} = \Delta P_{20} - \Delta P_{20}^{th} \end{cases} \tag{4.1}$$

where E is the surface evapotranspiration, $\alpha = 0.07K^{-1}$ at temperatures typical of the lower troposphere and represents the increase of the saturation vapor pressure, and $\langle \cdot \rangle$ indicates the mean value between the year $t - 20$ and t. A more detailed calculation with all hypotheses described is developed in "Appendix 3".

Table 2 Spatial boundaries of the four selected SREX regions

Region name	Mediterranean S.	Central America	South Asia	Arctic	Global average	
Acronym	MED ⊖	CAM ⊖	SAS ⊕	ARC ⊕	⊖	⊕
Region Boundaries	30N–10W 45N–10W 45N–40E 30N–40E	11.5N–69W 1S–79.5W 28.5N–118.5W 28.5N–90.5W	5N–60E 30N–60E 30N–100E 20N–100E 20N–95E 5N–95E	75N–180E 90N–180E 90N–180W 75N–180W		
1995-ratio	1.77 ± 0.27	2.01 ± 0.58	1.66 ± 0.32	1.61 ± 0.19	1.26 ± 0.09	1.40 ± 0.10
In 2080				land →	1.38 ± 0.15	1.33 ± 0.11
				ocean →	1.25 ± 0.09	1.39 ± 0.10

1995-ratio of the moistening (drying) rate in 2080. Error margins represent one σ-interval of the total year-to-year variability (natural and inter-model)

The first component of the thermodynamic term represents the evolution of surface evapotranspiration. The second component results from impacts of the Clausius–Clapeyron relationship on water availability in the climate system as temperature rises. The dynamic variation is associated with changes in the large-scale atmospheric circulation that result from two main influences: the direct effect of CO_2 on large-scale vertical motion, and the response of the circulation to surface temperature changes (Joshi et al. 2008; Cao et al. 2012; Bony et al. 2013).

The thermodynamic component is associated with a robust 'wet get wetter—dry get drier' pattern in all models (e.g. Polson et al. 2013) and is expected to scale with the global-mean temperature. The dynamic component exhibits a more complex pattern which can differ substantially across models (Bony et al. 2013). Therefore, the persistence of rate patterns over the same regions may result from the increasing prominence of the thermodynamic component ΔP_{20}^{th} (and thus of its robust 'wet-get-wetter, dry-get-drier' pattern) relative to the dynamic component ΔP_{20}^{dyn}. We test this hypothesis by diagnosing the relative contributions of ΔP_{20}^{dyn} and ΔP_{20}^{th} to the total rate over oceans. This analysis is performed with all four realizations of the IPSL-CM5A-LR model, which displays similar results as the multi-model mean (not shown).

In the projections, ΔP_{20} is dominated by the thermodynamic component (Fig. 8a), which closely follows ΔT_{20} (Chavaillaz et al, submitted). The dynamic component does not contribute much to ΔP_{20}, but it dominates the moistening and drying trends (Fig. 8b, c). It confirms that the precipitation trend is associated in any given region by a circulation change, either a change in intensity or a shift (Bony et al. 2004, 2013; Liu and Allan 2013).

The relative weight Φ_{dyn}^{-} of the dynamic component over the total variation of ΔP_{20}^{-} is defined as:

$$\Phi_{dyn}^{-} = \frac{\left|\Delta P_{20}^{dyn-}\right|}{\left|\Delta P_{20}^{th-}\right| + \left|\Delta P_{20}^{dyn-}\right|} \cdot 100 \tag{4.2}$$

Φ_{dyn}^{+} is similarly defined with ΔP_{20}^{+}. The weight of the dynamic contribution is strong, but stabilizes to current values over the century under RCP8.5, or even weakens (Fig. 8d, e). This is due to an increasing warming and a stronger influence of thermodynamic processes (Bony et al. 2013). This behavior is not seen under RCP2.6 because of the small projected temperature rise, and returns to historical values at the end of the century.

In other words, as global warming is accelerating, the relative weight of the dynamic component in drying and moistening regions decreases relative to the growing thermodynamic term. Thus, it tends to stabilize spatial rate patterns of precipitation change. This mechanism can also be responsible for the stable ratio of 60/40 % of moistening/drying regions. Atmospheric cells might indeed not expand because of the decreasing weight of dynamic contributions.

4.2 Extension to land surfaces

By definition, the dynamic component of precipitation change is due to change in ω, the pressure vertical velocity (see "Appendix 3"). To further support the increasing contribution of thermodynamic processes at the global scale and not only over oceans, we define the *fraction of switching regions relative to* $\Delta\omega_{20}$, the rate of change of ω at 500 hPa. We use this indicator as a proxy for stabilization of circulation patterns. Its global evolution is illustrated in Fig. 9a with oceans and land surfaces taken together. This fraction strongly decreases under RCP8.5 (unlike RCP2.6), meaning that regions exhibiting an increase (or a decrease) of ascendence also tend to become more geographically

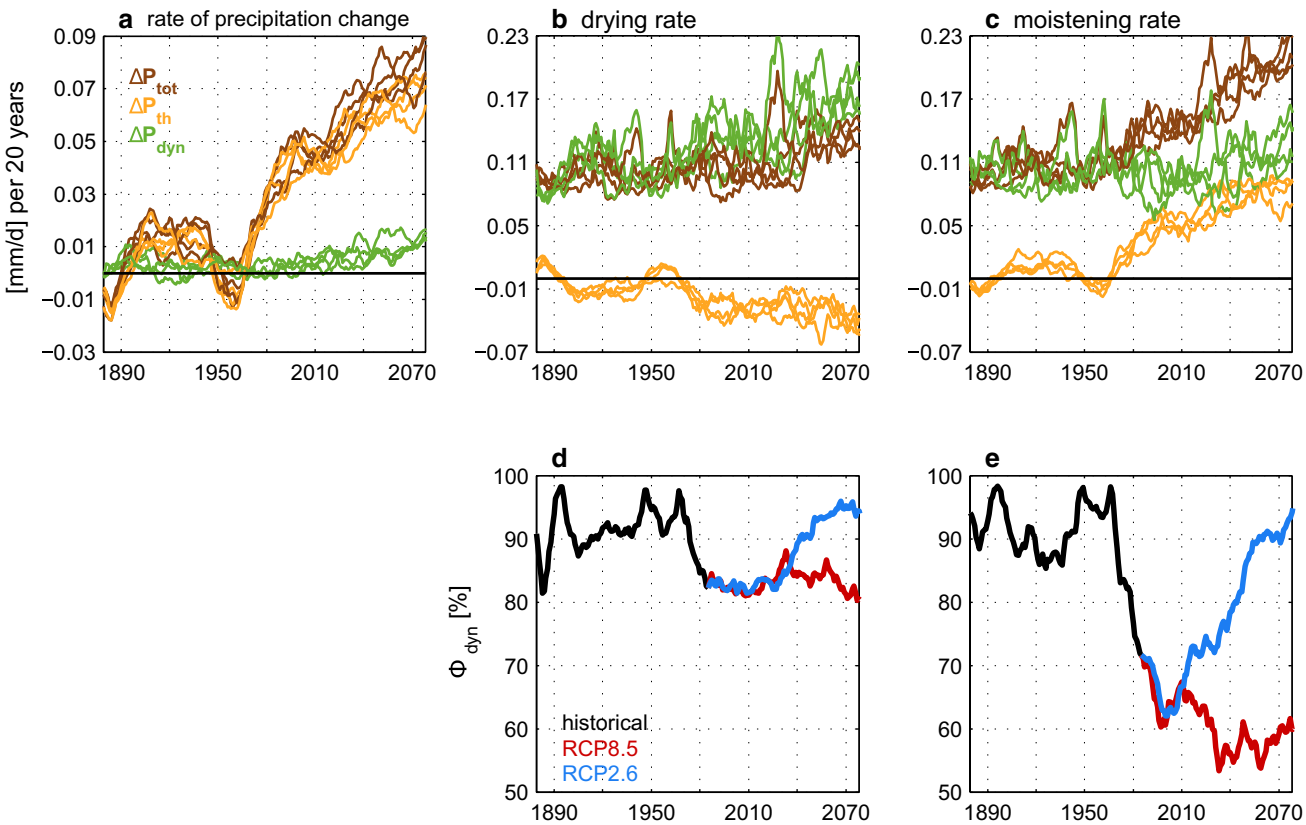

Fig. 8 Evolution of the thermodynamic (*orange*) and dynamic (*green*) components of **a** the rate of precipitation change, **b** the drying rate, and **c** the moistening rate compared with the sum of both contributions (*brown*) under the RCP8.5 scenario. Each *curve* represents one out of four realizations of the IPSL-CM5A-LR model. Evolution of the contribution Φ_{dyn} of the dynamic component to the total value of **d** the drying rate and **e** the moistening rate in multi-realization mean values of IPSL-CM5A-LR for the historical, RCP2.6 and RCP8.5 experiments

stationary. Therefore, the significant decrease is firstly linked to a declining relative weight of dynamic processes in ΔP_{20} and then, to a slowdown of the expansion of Hadley-Walker cells explaining the stable predominance of moistening regions. A similar evolution is displayed when selecting land surfaces separately (Fig. 9b). A robust 'dry gets drier, wet gets wetter' pattern is shown only on 10 % of the global land area during the second half of the twentieth century (Greve et al. 2014), and such a pattern is not projected over all land areas in a future under strong emissions (Byrne and O'Gorman 2015). But we show here that it has already started to expand, and might substantially expand further.

5 Discussion

5.1 Summary of key findings

We suggest here an alternative approach to characterize projections of future precipitation change under global warming. Instead of using a fixed-current baseline as a reference period, a running reference is adopted, illustrating projected changes relative to the previous two decades. Several key indicators are defined in order to describe the rate at which precipitation regimes change under global warming: the rate of precipitation change ΔP_{20}, the moistening (drying) rate ΔP_{20}^{+} (ΔP_{20}^{-}), the fraction of moistening (drying) regions Π_{+} (Π_{-}) and the fraction of switching regions Π_{s20} going from a moistening to a drying or vice versa.

Under the strongest emission pathway corresponding to an absence of mitigation policies over several coming decades (RCP8.5), the annual rate of precipitation change keeps increasing continuously at the global scale, resulting in a doubling of the rate of change in mean precipitation by 2080 compared to the present day. Regions with significant rate patterns strongly expand over land surfaces as well as over oceans, while moving further from the current period. Moistening regions are in stable predominance ($\simeq 60\,\%$). The main new finding is that significant rate patterns tend to become more geographically stationary, increasing the

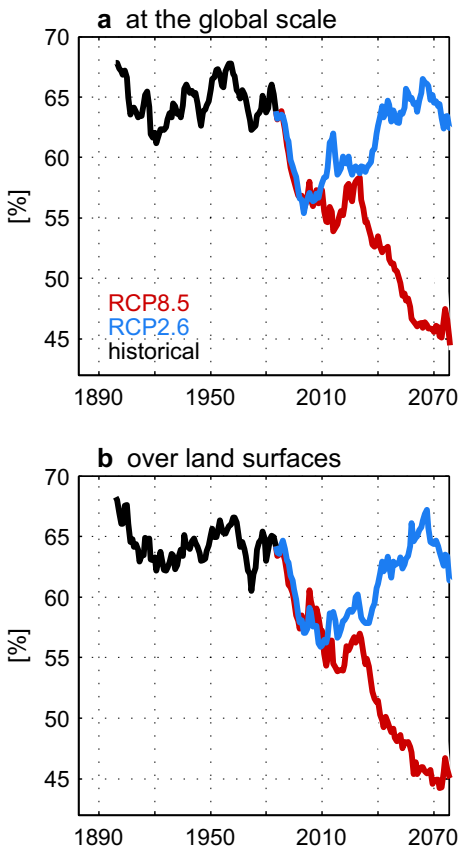

Fig. 9 Evolution of the fraction of switching regions relative to $\Delta\omega_{20}$ **a** at the global scale and **b** over land surfaces in multi-realization mean values with the IPSL-CM5A-LR model for RCP8.5, RCP2.6 and the historical experiment

persistence of trends over the same regions. Indeed, switching regions drop from 65 % during the historical period to 40 % by the end of the twenty-first century in multi-model mean values. Whilst temperature rise is accelerating, this stabilization is due to the increasing weight of thermodynamic processes in controlling precipitation changes.

The combination of intensification and persistence of such substantial rates might have strong impacts on human and natural systems (e.g. in the Mediterranean basin, Central America, South Asia and the Arctic). These regions even exhibit a larger rate and a larger increase of rate over the century compared to the global scale. For instance, the drying trend of Central America, mostly due to an attenuation of the summer wet season, is projected to be twice as fast by 2080 compared to the current period ($R_- = 2.01 \pm 0.58$), whereas the global average of the 1995-ratio in the drying rate is displayed to be about 1.26 ($\pm$0.09).

In contrast, under the strongest mitigation pathway (RCP2.6), evolution of all indicators is similar with RCP8.5 until 2010 (i.e. until the 2011–2030 period). These indicators return to historical values for the rest of the twenty-first century: after a sudden decrease in the fraction of switching regions (65–53 %), it is predicted to go back to initial values. The moistening and drying rates are nearly constant. The fraction of moistening regions goes back to about 50 %, loosing their predominance. All the critical phenomena described here for RCP8.5 might not happen if strong mitigation policies are quite rapidly implemented.

5.2 Limitations of the study

This work consists of a multi-model and multi-realization analysis involving CMIP5 simulations of 18 GCMs. Precipitation is one of the key variables to assess in a context of climate change. However, model projections of surface air temperature are of better quality than for precipitation (Flato et al. 2013). Daily precipitation statistics improve with increasing spatial resolution (e.g. Boberg et al. 2009, 2010), but sub-daily statistics reveal important challenges, especially concerning the diurnal cycle (Dai and Trenberth 2004; Dai 2006). Higher time resolution in precipitation statistics are also needed (e.g. Haerter et al. 2010), especially for evaluation of convective precipitation. This is the reason why we compare the simulated rate of precipitation change with the one inferred from available observation and reanalysis datasets, in order to evaluate its robustness.

On one hand, we know models have limitations in simulating precipitation, and that applies to reanalysis as well. They are not designed to represent the timing of unforced variability, and a misrepresentation of natural forcing might explain some of the differences to the observations. But on the other hand, the observed precipitation trend over the twentieth century can exhibit a relative uncertainty about 50–100 %, and even more than 100 % when limited to the second half of the century (Hartmann et al. 2013). It may be caused by different factors, including instrumental problems, precipitation undercatch, and station versus grid cell comparison. Spatial and year-to-year variability also constitutes an important part of the limits of a multi-model precipitation analysis, especially at the regional scale. Natural variability plays a non-negligible role, but inter-model variability has an even greater influence. Indeed, models exhibit a large spread, mainly because of precipitation change caused by dynamic processes (Flato et al. 2013). However, focusing on regions that exhibit a robust change across GCMs allows the relative contribution of inter-model variability to be reduced, producing reliable information for impact studies. Despite these two major shortcomings in simulated precipitation (i.e. discrepancies with observations and large variability), GCM output remains the best source of information concerning possible evolution of precipitation changes, and is qualitatively robust.

While the rate of change of mean precipitation may be of importance to adaptation (Klein et al. 2014), impacts are also determined by precipitation extremes, thresholds, timing and characteristics of the wet season and multi-year drought, and evaporation and soil moisture over land controlling the water stress. All these characteristics are not included in this analysis. Therefore, all derived interpretations require some caution. In the next subsection, we allow ourselves to draw some conclusions regarding the evolution of rate of change indicators related to precipitation may have on climate impacts and adaptation communities, keeping in mind that risk also depends on vulnerability and exposure of human and natural systems and not just on climate hazards (IPCC 2014).

5.3 Main implications

This study distinguishes itself by focusing on projected precipitation changes with a moving baseline. The increasing weight of thermodynamic processes in controlling precipitation changes has also been highlighted using a fixed-current baseline, and a separation between dry and wet regimes, instead of drying and moistening regimes (Liu and Allan 2013). We bring here additional relevant information about the quantification of the persistence of significant rate patterns directly linked to these processes. Greve et al. (2014) demonstrated that a 'dry gets drier and wet gets wetter' pattern was uncommon over land during the historical period considering a Budyko framework. But considering another framework, we show that this pattern has already started to expand, and might get more usual in a future under strong emissions. Roderick et al. (2012) stated that the behavior of the water cycle is different over land and ocean, but we highlight here one of the mechanisms of precipitation change that are similar over all surfaces.

By describing changes from one 20-year period to the next, our approach could also be a good starting point to more concretely represent what future generations might experience. The memory of climate and weather events is indeed often limited to an average generation (Garnier 2010). Using alternative time horizons might assess how they may react and adapt regarding future precipitation change (de Elía et al. 2014). An intensification of rate in regions with a significant and persistent rate pattern may give less time for human and natural systems to adapt (O'Neill and Oppenheimer 2004). Additional effort might be needed compared to recent adaptation. Our approach has demonstrated that significant and persistent rate patterns will expand and increase in their amplitude in a future under strong emissions, and thus might bring out relevant insights for climate impacts and adaptation communities.

Acknowledgments We acknowledge the World Climate Research Programme's Working Group on Coupled Modelling, which is in charge of the fifth Coupled Model Intercomparison Project, and we thank the climate modelling groups for producing and making available their model output. To analyze the CMIP5 data, this study benefited from the IPSL Prodiguer-Ciclad facility which is supported by CNRS, UPMC, Labex L-IPSL which is funded by the ANR (Grant # ANR-10-LABX-0018) and by the European FP7 IS-ENES2 project (Grant #312979). We especially thank S. Denvil and J. Raciazek for supervising data fetching. We also warmly acknowledge L. Terray at CERFACS in Toulouse, R. Knutti at ETH Zürich, and the two anonymous reviewers for their comments and constructive suggestions on our work. This study is accomplished as part of a PhD thesis equally funded by the French Alternative Energies and Atomic Energy Commission (CEA) and the French Ministry of Defense (DGA). We thus acknowledge both organizations for making this work possible.

Author contributions Y.C. and S.J. coordinated the study. Y.C. wrote the paper, developed and performed analyses. All the authors discussed the results and their interpretation and contributed to the final version of the paper.

Appendix 1: Additivity of precipitation rates

In order to preserve additivity of both drying and moistening rates, the computation of multi-model mean values is conducted as follows. For each model l, each realization r and each year t, ΔP_{20} is expressed as:

$$\Delta P_{20} = \Pi_+ \cdot \Delta P_{20}^+ - \Pi_- \cdot \Delta P_{20}^- \tag{6.1}$$

where Π_+ (Π_-) is the fraction of moistening (drying) regions.

To ensure that Eq. (6.1) is valid for multi-model mean values, the multi-model means of the drying and moistening rates are weighted by the fraction of drying and moistening regions:

$$\begin{cases} \overline{\Delta P_{20}^+}^{l,r} = \dfrac{\sum_{l,r}\left(\Pi_{+,l,r} \cdot \Delta P_{20,l,r}^+\right)}{\sum_{l,r} \Pi_{+,l,r}} \\ \overline{\Delta P_{20}^-}^{l,r} = \dfrac{\sum_{l,r}\left(\Pi_{-,l,r} \cdot \Delta P_{20,l,r}^-\right)}{\sum_{l,r} \Pi_{-,l,r}} \end{cases} \tag{6.2}$$

with $\overline{\cdots}^{l,r}$ representing the average of all models and all realizations, i.e. the multi-model mean.

Appendix 2: Additive conditions of natural and inter-model variability

Indicators are computed with L models including R_l realizations. Raw prediction X for each model l, realization r and year t can be expressed as:

$$X_{l,r,t} = x_t + x'_{l,t} + \varepsilon_{l,r,t} \tag{7.1}$$

where x_t is the multi-model mean value, $x'_{l,t}$ is the difference between x_t and the multi-realization mean value of each model and $\varepsilon_{l,r,t}$ is the difference between the multi-run mean value of the considered model and $X_{l,r,t}$.

Within the scope of this work, we consider two hypotheses:

H1 The *inter-model* and *natural* variabilities are two independent processes, which is true as a first approximation and is an assumption of this analysis.

H2 The multi-realization mean $\overline{\varepsilon_{l,r,t}}^r$ of $\varepsilon_{l,r,t}$ for each model l and each time t equals zero, which is true by definition of the multi-realization mean.

The natural variability $\sigma^2_{R,l}$ for each model l is defined as the temporal variance of $\varepsilon_{l,r,t}$. It is time- and realization-independent for each model. The multi-model mean σ^2_R of $\sigma^2_{R,l}$ is computed in accordance with an equal weight amongst all models. The inter-model variability $\sigma^2_{L,t}$ is estimated from the variance between multi-realization mean values of each model at each time step and is thus time dependent. In the following calculation, we give an equal weight to each run for simplicity, whatever the model or the realization. The final results of the calculation remain identical. The total variability of the indicator is computed using Eq. (7.1) as follows:

$$\begin{aligned}\sigma^2_{T,t} &= \mathrm{Var}_{l,r}\left(X_{l,r,t}\right)\\ &= \frac{1}{L}\sum_l\left[\frac{1}{R_l}\sum_r\left(X_{l,r,t}-x_t\right)^2\right]\\ &\overset{(B.1)}{=} \frac{1}{L}\sum_l\left[\frac{1}{R_l}\sum_r\left(x'^2_{l,t}+2x'_{l,t}\cdot\varepsilon_{l,r,t}+\varepsilon^2_{l,r,t}\right)\right]\\ &= \overline{x'^2_{l,t}}^l + 2\cdot\overline{x'_{l,t}\cdot\overline{\varepsilon_{l,r,t}}^r}^l + \overline{\varepsilon^2_{l,r,t}}^{l,r}\\ &\overset{(H2)}{=} \overline{x'^2_{l,t}}^l + \overline{\varepsilon^2_{l,r,t}}^{l,r}\end{aligned} \tag{7.2}$$

$\sigma^2_{L,t}$ and σ^2_R can be expressed the same way:

$$\begin{aligned}\sigma^2_{L,t} &= \mathrm{Var}_l\left(x_t+x'_{l,t}\right)\\ &= \frac{1}{L}\sum_l\left(x_t+x'_{l,t}-x_t\right)^2\\ &= \overline{x'^2_{l,t}}^l\end{aligned} \tag{7.3}$$

$$\begin{aligned}\sigma^2_R &= \frac{1}{L}\sum_l\left[\frac{1}{R_l}\sum_r\mathrm{Var}_{r,t}\left(\varepsilon_{l,r,t}\right)\right]\\ &= \frac{1}{L}\sum_l\left[\frac{1}{R_l}\sum_r\left(\varepsilon_{l,r,t}-\overline{\varepsilon_{l,r,t}}^{r,t}\right)^2\right]\\ &= \overline{\varepsilon^2_{l,r,t}-2\varepsilon_{l,r,t}\cdot\overline{\varepsilon_{l,r,t}}^{r,t}+\left(\overline{\varepsilon_{l,r,t}}^{r,t}\right)^2}^{l,r}\\ &\overset{(H2)}{=} \overline{\varepsilon^2_{l,r,t}}^{l,r}\end{aligned} \tag{7.4}$$

The total variability is the sum of both natural and inter-model variabilities:

$$\sigma^2_{T,t} = \sigma^2_R + \sigma^2_{L,t} \tag{7.5}$$

The additivity of σ^2_R and $\sigma^2_{L,t}$ is thus the direct consequence of the way we constructed the decomposition of each source of uncertainty.

Appendix 3: Detailed calculation of the (thermo) dynamic components of ΔP_{20}

The vertically integrated water budget can be diagnosed regionally as follows for each GCM, each run and each yearly mean value (Neelin 2007; Bony et al. 2013):

$$P = E - \left[q\nabla\cdot\mathbf{V}\right] - \left[\mathbf{V}\cdot\nabla q\right] \tag{8.1}$$

where P is the precipitation, E the surface evapotranspiration, $\mathbf{V}$ the field of horizontal wind velocity and q the vertical profile of specific humidity. The vertically integrated horizontal moisture advection term $-\left[\mathbf{V}\cdot\nabla q\right]$ is hereafter denoted as H_q. Mass continuity can be expressed as:

$$\nabla\cdot\mathbf{V} + \frac{\partial\omega}{\partial\tilde{p}} = 0 \tag{8.2}$$

where ω is the pressure vertical velocity and $\tilde{p}$ the atmospheric pressure. Considering that $\omega = 0$ at the Earth surface and at the top of the atmosphere, a vertical integration by parts leads to:

$$\frac{\mathrm{d}(\omega q)}{\mathrm{d}\tilde{p}} = \omega\frac{\partial q}{\partial\tilde{p}} + q\frac{\partial\omega}{\partial\tilde{p}} = \omega q\big|_{\tilde{p}_{surf}}^{\tilde{p}_{toa}} = 0 \tag{8.3}$$

The combination of (8.2) and (8.3) implies that a variation of (8.1) is expressed as:

$$\Delta P = \Delta E - \Delta\left[\omega\frac{\partial q}{\partial\tilde{p}}\right] + \Delta H_q \tag{8.4}$$

As the dynamic contribution in precipitation changes is only caused by global circulation changes (i.e. variation of ω), (8.4) can be formulated differently:

$$\Delta P = \underbrace{\Delta E - \omega\Delta\left[\frac{\partial q}{\partial\tilde{p}}\right] + \Delta H_q}_{\Delta P_{th}} + \underbrace{\left[\frac{\partial q}{\partial\tilde{p}}\right]\Delta\omega}_{\Delta P_{dyn}} \tag{8.5}$$

On the other hand, the Clausius–Clapeyron expression for vapor saturation is (e.g. Held and Soden 2006):

$$\frac{\mathrm{d}\ln q}{\mathrm{d}T} = \frac{L}{RT^2} = \alpha(T) \tag{8.6}$$

where T is the surface air temperature, L the latent heat of vaporization and R the gas constant. At temperatures

corresponding to those of the lower troposphere, $\alpha = 0.07K^{-1}$ above oceans. Then, (8.6) becomes:

$$\mathrm{d}q = 0.07q \cdot \mathrm{d}T \tag{8.7}$$

Using the vertically integrated water budget (8.1) and the Clausius–Clapeyron relation (8.7) in (8.5), we obtain:

$$\Delta P = \Delta E + 0.07(P - E)\Delta T + \Delta P_{dyn} \tag{8.8}$$

This expression is a valid approximation for absolute change of precipitation above oceans, but also for a running difference with the only condition that $P = \langle P \rangle_{t,t-20}$ and $E = \langle E \rangle_{t,t-20}$, the mean of annual precipitation (evapotranspiration) during the last twenty years. The rate of precipitation change ΔP_{20} as well as the moistening (drying) rates ΔP_{20}^{+} (ΔP_{20}^{-}) can be split in two distinctive parts coming from thermodynamic and dynamic modifications of the atmosphere:

$$\begin{cases} \Delta P_{20}^{th} = \Delta E_{20} + 0.07(\langle P \rangle - \langle E \rangle)\Delta T_{20} \\ \Delta P_{20}^{dyn} = \Delta P_{20} - \Delta P_{20}^{th}. \end{cases} \tag{8.9}$$

References

Allan RP (2012) Regime dependent changes in global precipitation. Clim Dyn 39(3–4):827–840. doi:10.1007/s00382-011-1134-x

Allan RP, Liu M, Cand Z, Lavers DA, Koukouvagias E, Bodas-Salcedo A (2014) Physically consistent responses of the global atmospheric hydrological cycle in models and observations. Surv Geophys 35(3):533–552. doi:10.1007/s10712-012-9213-z

Becker A, Finger P, Meyer-Christoffer A, Rudolf B, Schamm K, Schneider U, Ziese M (2013) A description of the global land-surface precipitation data products of the global precipitation climatology centre with sample applications including centennial (trend) analysis from 1901 to present. Earth Syst Sci Data 5(1):71–99. doi:10.5194/essd-5-71-2013

Boberg F, Berg P, Thejll P, Gutowski WJ, Christensen JH (2009) Improved confidence in climate change projections of precipitation evaluated using daily statistics from the PRUDENCE ensemble. Clim Dyn 32(7–8):1097–1106. doi:10.1007/s00382-008-0446-y

Boberg F, Berg P, Thejll P, Gutowski WJ, Christensen JH (2010) Improved confidence in climate change projections of precipitation further evaluated using daily statistics from ENSEMBLES models. Clim Dyn 35(7–8):1509–1520. doi:10.1007/s00382-009-0683-8

Bony S, Dufresne JL, Le Treut H, Morcrette JJ, Senior C (2004) On dynamic and thermodynamic components of cloud changes. Clim Dyn 22(2–3):71–86. doi:10.1007/s00382-003-0369-6

Bony S, Bellon G, Klocke D, Sherwood S, Fermepin S, Denvil S (2013) Robust direct effect of carbon dioxide on tropical circulation and regional precipitation. Nat Geosci 6(6):447–451. doi:10.1038/ngeo1799

Byrne MP, O'Gorman PA (2015) The response of precipitation minus evapotranspiration to climate warming: why the "wet-get-wetter, dry-get-drier" scaling does not hold over land. J Clim 28(20):8078–8092. doi:10.1175/JCLI-D-15-0369.1

Cao L, Bala G, Caldeira K (2012) Climate response to changes in atmospheric carbon dioxide and solar irradiance on the time scale of days to weeks. Environ Res Lett 7(034):015. doi:10.1088/1748-9326/7/3/034015

Chadwick R, Boutle I, Martin G (2013) Spatial patterns of precipitation change in CMIP5: why the rich do not get richer in the tropics. J Clim 26(11):3803–3822. doi:10.1175/JCLI-D-12-00543.1

Chapin FS et al (2000) Consequences of changing biodiversity. Nature 405(6783):234–242. doi:10.1038/35012241

Chavaillaz Y, Joussaume S, Dehecq A, Braconnot P, Vautard R (submitted) Investigating the pace of temperature change and its implications over the twenty-first century. Clim Change

Chou C, Chiang JCH, Lan CW, Chung CH, Liao YC, Lee CJ (2013) Increase in the range between wet and dry season precipitation. Nat Geosci 6(4):263–267. doi:10.1038/ngeo1744

Collins M et al (2013) Long-term climate change: projections, commitments and irreversibility. In: Climate Change 2013: the physical science basis. Contribution of working group I to the fifth assessment report of the intergovernmental panel on climate change, Cambridge University Press

Dai A (2006) Precipitation characteristics in eighteen coupled climate models. J Clim 19(18):4605–4630. doi:10.1175/JCLI3884.1

Dai A, Trenberth KE (2004) The diurnal cycle and its depiction in the community climate system model. J Clim 17(5):930–951. doi:10.1175/1520-0442

Dawson TP, Jackson ST, House JI, Prentice IC, Mace GM (2011) Beyond predictions: biodiversity conservation in a changing climate. Science 332(6025):53–58. doi:10.1126/science.1200303

Deser C, Phillips A, Bourdette V, Teng H (2010) Uncertainty in climate change projections: the role of internal variability. Clim Dyn 38:527–546. doi:10.1007/s00382-010-0977-x

de Elía R, Biner S, Frigon A, Côté H (2014) Timescales associated with climate change and their relevance in adaptation strategies. Clim Change 126(1–2):93–106. doi:10.1007/s10584-014-1209-x

Flato G, et al (2013) Evaluation of climate models. In: Climate Change 2013: the physical science basis. Contribution of working group I to the fifth assessment report of the intergovernmental panel on climate change, Cambridge University Press

Garnier E (2010) Les dérangements du temps, 500 ans de chaud et froids en Europe. Plon

Giorgi F, Bi X (2009) Time of emergence (ToE) of GHG-forced precipitation change hot-spots. Geophys Res Lett 36(6):L06,709. doi:10.1029/2009GL037593

Greve P, Orlowsky B, Mueller B, Sheffield J, Reichstein M, Seneviratne SI (2014) Global assessment of trends in wetting and drying over land. Nat Geosci 7(10):716–721. doi:10.1038/ngeo2247

Haerter JO, Berg P, Hagemann S (2010) Heavy rain intensity distributions on varying time scales and at different temperatures. J Geophys Res Atmos 115(D17). doi:10.1029/2009JD013384

Harris I, Jones P, Osborn T, Lister D (2014) Updated high-resolution grids of monthly climatic observations—the CRU TS3.10 dataset. Int J Climatol 34(3):623–642. doi:10.1002/joc.3711

Hartmann DL et al (2013) Observations: atmosphere and surface. In: Climate Change 2013: the physical science basis. Contribution of working group I to the fifth assessment report of the intergovernmental panel on climate change, Cambridge University Press

Hawkins E, Sutton R (2009) The potential to narrow uncertainty in regional climate predictions. Bull Am Meteorol Soc 90:1095–1107. doi:10.1175/2009BAMS2607.1

Hawkins E, Sutton R (2011) The potential to narrow uncertainty in projections of regional precipitation change. Clim Dyn 37(1–2):407–418. doi:10.1007/s00382-010-0810-6

Held IM, Soden BJ (2006) Robust responses of the hydrological cycle to global warming. J Clim 19(21):5686–5699. doi:10.1175/JCLI3990.1

IPCC (2014) Summary for policymakers. In: Climate Change 2014: impacts, adaptation, and vulnerability. Part A: global and sectoral aspects. Contribution of working group II to the fifth assessment report of the intergovernmental panel on climate change, Cambridge University Press, pp 1–32

Ji F, Zhaohua W, Jianping H, Chassignet EP (2014) Evolution of land surface air temperature trend. Nat Clim Change 4(6):462–466. doi:10.1038/nclimate2223

Joshi M, Gregory J, Webb M, Sexton D, Johns T (2008) Mechanisms for the land/sea warming contrast exhibited by simulations of climate change. Clim Dyn 30(5):455–465. doi:10.1007/s00382-007-0306-1

Kirtman B et al (2013) Near-term climate change: projections and predictability. In: Climate Change 2013: the physical science basis. Contribution of working group I to the fifth assessment report of the intergovernmental panel on climate change, Cambridge University Press

Klein RJT et al (2014) Adaptation opportunities, constraints, and limits. In: Climate Change 2014: impacts, adaptation, and vulnerability. Part A: global and sectoral aspects. Contribution of working group II to the fifth assessment report of the intergovernmental panel on climate change, Cambridge University Press, pp 899–943

Liebmann B, Dole RM, Jones C, Bladé I, Allured D (2010) Influence of choice of time period on global surface temperature trend estimates. Bull Am Meteorol Soc 91(11):1485–1491. doi:10.1175/2010BAMS3030.1

Liu C, Allan RP (2013) Observed and simulated precipitation responses in wet and dry regions 1850–2100. Environ Res Lett 8(3):034,002. doi:10.1088/1748-9326/8/3/034002

Mahlstein I, Portmann RW, Daniel JS, Solomon S, Knutti R (2012) Perceptible changes in regional precipitation in a future climate. Geophys Res Lett 39(L05):701. doi:10.1029/2011GL050738

Maraun D (2013) When will trends in European mean and heavy daily precipitation emerge? Environ Res Lett 8(1):014,004. doi:10.1088/1748-9326/8/1/014004

Masson-Delmotte V et al (2013) Information from paleoclimate archives. In: Climate Change 2013: the physical science basis. Contribution of working group I to the fifth assessment report of the intergovernmental panel on climate change, Cambridge University Press

Meinshausen M, Smith S, Calvin K, Daniel J, Kainuma M, Lamarque JF, Matsumoto K, Montzka S, Raper S, Riahi K, Thomson A, Velders G, van Vuuren D (2011) The RCP greenhouse gas concentrations and their extensions from 1765 to 2300. Clim Change 109(1–2):213–241. doi:10.1007/s10584-011-0156-z

Mora C, Frazier AG, Longman RJ, Dacks RS, Walton MM, Tong EJ, Sanchez JJ, Kaiser LR, Stender YO, Anderson JM, Ambrosino CM, Fernandez-Silva I, Giuseffi LM, Giambelluca TW (2013) The projected timing of climate departure from recent variability. Nature 502(7470):183–187. doi:10.1038/nature12540

Neelin JD (2007) Moist dynamics of tropical convection zones in monsoons, teleconnections, and global warming. In: Schneider T, Sobel A (eds) The global circulation of the atmosphere. Princeton University Press, Princeton, pp 267–301

Neelin JD, Münnich M, Su H, Meyerson JE, Holloway CE (2006) Tropical drying trends in global warming models and observations. Proc Nat Acad Sci 103(16):6110–6115. doi:10.1073/pnas.0601798103

O'Neill BC, Oppenheimer M (2004) Climate change impacts are sensitive to the concentration stabilization path. Proc Nat Acad Sci 101(47):16,411–16,416. doi:10.1073/pnas.0405522101

Poli P, Hersbach H, Tan D, Dee D, Thépaut JN, Simmons A, Peubey C, Laloyaux P, Komori T, Berrisford P, Dragani R, Trémolet Y, Holm E, Bonavita M, Isaksen L, Fisher M (2013) The data assimilation system and initial performance evaluation of the ECMWF pilot reanalysis of the twentieth century assimilating surface observations only (ERA-20C). ERA Report Series (14)

Polson D, Hegerl GC, Allan RP, Sarojini BB (2013) Have greenhouse gases intensified the contrast between wet and dry regions? Geophys Res Lett 40(17):4783–4787. doi:10.1002/grl.50923

Roderick ML, Sun F, Farquhar GD (2012) Water cycle varies over land and sea. Science 336(6086):1230–1231. doi:10.1126/science.336.6086.1230-b

Seneviratne SI et al (2012) Changes in climate extremes and their impacts on the natural physical environment. In: Managing the risks of extreme events and disasters to advance climate change adaptation. A special report of working groups I and II of the intergovernmental panel on climate change (IPCC), Cambridge University Press

Settele J, et al (2014) Terrestrial and inland water systems. In: Climate Change 2014: impacts, adaptation, and vulnerability. Part A: global and sectoral aspects. Contribution of working group II to the fifth assessment report of the intergovernmental panel on climate change, Cambridge University Press, pp 195–228

Smith SJ, Edmonds J, Hartin CA, Mundra A, Calvin K (2015) Near-term acceleration in the rate of temperature change. Nat Clim Change 5:333–336. doi:10.1038/nclimate2552

Street R, Jacob D, Parry M, Runge T, Scott J (2015) A European research and innovation roadmap for climate services. European Commission. doi:10.2777/702151

Taylor KE, Stouffer RJ, Meehl GA (2011) An overview of CMIP5 and the experiment design. Bull Am Meteorol Soc 93(4):485–498. doi:10.1175/BAMS-D-11-00094.1

Vecchi GA, Soden BJ (2007) Global warming and the weakening of the tropical circulation. J Clim 20(17):4316–4340. doi:10.1175/JCLI4258.1

Vose RS, Schmoyer RL, Steurer PM, Peterson TC, Heim R, Karl TR, Eischeid JK (1992) The global historical climatology network: long-term monthly temperature, precipitation, sea level pressure, and station pressure data. Oak Ridge National Laboratory. doi:10.3334/CDIAC/cli.ndp041

Zhang X, Zwiers FW, Hegerl GC, Lambert FH, Gillett NP, Solomon S, Stott PA, Nozawa T (2007) Detection of human influence on twentieth-century precipitation trends. Nature 448(7152):461–465. doi:10.1038/nature06025